Sensors and Materials, Vol. 32, No. 4 (2020) 1365–1372
MYU Tokyo

S & M 2182

X-ray-induced Scintillation via Energy Transfer from Gd^{3+} to Ce^{3+} in Silicate Glasses Composed of Heavy Elements

Daiki Shiratori,* Daisuke Nakauchi, Takumi Kato,
Noriaki Kawaguchi, and Takayuki Yanagida

Nara Institute of Science and Technology, 8916-5 Takayama, Ikoma, Nara 630-0192, Japan

(Received December 16, 2019; accepted February 28, 2020)

Keywords: glass scintillator, energy transfer, silicate glass, scintillation

Photoluminescence and X-ray-induced scintillation properties of xCe:20BaO-15Gd_2O_3-65SiO_2 (x = 0, 0.01, 0.05, 0.1, 0.5) glasses were investigated. The glass samples emitted light via energy transfer from Gd^{3+} in the host to Ce^{3+}. The $^6P_{7/2}$–$^8S_{7/2}$ relaxation of Gd^{3+} was confirmed notably in the undoped glass sample, but the emission due to Gd^{3+} disappeared upon the addition of Ce. Furthermore, the decay time constant of Gd^{3+} decreased with increasing Ce concentration.

1. Introduction

The development of new scintillators is required for industrial and medical imaging applications,[1–6] high-energy and nuclear physics,[7–10] and security fields.[11–13] Recently, glasses have become attractive materials owing to their prominent advantages, such as low cost and easy formability, and these advantages are preferable for manufacturing scintillators. However, glass scintillators suffer from a rather low energy transfer efficiency under ionizing radiation irradiation, which results in a low light yield compared with crystals.[14] In addition, most developed glass scintillators including the ^{6}Li-glass are mainly composed of light elements;[15–18] therefore, they have a low interaction probability with X- or γ-rays.

To obtain a high density of samples, which is directly associated with high detection efficiency against X- or γ-rays,[19,20] considerable attention has been paid to Ce^{3+}- or Tb^{3+}-doped glasses containing a large number of Gd as a host.[21–23] The number of Gd_2O_3 in some glasses can reach up to 30 mol% without phase separation.[24,25] Furthermore, in such high-Gd-containing glasses, Gd^{3+} ions enable efficient energy migration followed by single-step energy transfer towards emission centers.[26] Therefore, the light yield of Ce^{3+}-doped Gd-based glasses increases because of energy transfer from Gd^{3+} to Ce^{3+} when excited with UV or X-rays.[14,26]

Silicate glasses offer excellent properties such as transparency, chemical durability, thermal resistance, and high mechanical hardness. Because of these properties, silica glass has been widely applied commercially and industrially. Up to now, some silicate glasses have been developed for radiation detector applications, and they exhibit attractive detector properties.[27–32]

*Corresponding author: e-mail: shiratori.daiki.sc3@ms.naist.jp
https://doi.org/10.18494/SAM.2020.2740

ISSN 0914-4935

Therefore, in this study, we focused on SiO_2 and Gd_2O_3 as the main components of a host and Ce^{3+} as the luminescence center and investigated Ce-doped 20BaO-15Gd_2O_3-65SiO_2 glasses for scintillator applications.

2. Materials and Methods

2.1 Sample preparation

We prepared glass samples by the melt quenching method. Gd_2O_3 (4N), $BaCO_3$ (4N), and SiO_2 (5N) powders were used as raw materials, and the chemical composition of the host was 20BaO-15Gd_2O_3-65SiO_2. As luminescent centers, CeO_2 (4N) powder was introduced to the host of concentrations of 0, 0.01, 0.05, 0.1, and 0.5% in molar ratio against the entire host considered to be 100%. These powders 10.0 g in total were homogeneously mixed using an agate mortar. The mixture was transferred into an alumina crucible and pressed to suppress air bubbles in the glass. Then, the powder was melted in air atmosphere using an electric furnace at 1400 °C for 1 h. The melt was flowed out on a stainless-steel plate preheated to 300 °C and quenched. After sufficient cooling, the obtained glass samples were cut into dimensions of $5.80 \times (4.95 \pm 0.22) \times (1.55 \pm 0.14)$ mm^3. The glass samples were formed into similar shapes, and both top and bottom surfaces were polished. The densities of the glass samples were determined by the Archimedes method using analytical balances (GR-120, A&D Company, Limited).

2.2 Analysis method

Quantaurus-QY (C11347, Hamamatsu Photonics) was used to evaluate the photoluminescence (PL) excitation/emission contour maps and PL quantum yields (*QY*s). The monitoring excitation and emission wavelength ranges were 250–400 and 200–950 nm, respectively, with 10 nm intervals. A spectrophotometer (V670, JASCO) was operated to measure the absorption spectra across a spectral range from 190 to 2700 nm with 1 nm intervals. PL lifetime measurements were performed using Quantaurus-Tau (C11367, Hamamatsu Photonics).

We measured scintillation spectra using our laboratory-made setup.[33] We used an X-ray generator (XRB80N100/CB, Spellman) equipped with a conventional X-ray tube as the X-ray source and determined the operation current and tube voltage of the X-ray tube to be 1.2 mA and 40 kV, respectively. The scintillation obtained by X-ray irradiation was guided through an optical fiber to a monochromator equipped with a CCD-based detector (Shamrock 163 monochromator and DU-420-BU2 CCD, Andor).

Scintillation lifetimes were measured using a custom-made system.[34] This system adopted the time-correlated single-photon counting technique to evaluate the X-ray-induced scintillation lifetime. In this system, visible photons emitted from a light source hit a multi-alkali photocathode of an X-ray tube and were converted to photoelectrons. The generated photoelectrons were accelerated by a 30 kV high-voltage bias supplied by high-voltage power sources, and they collided with a W target. Then, bremsstrahlung X-rays were generated and

led to a sample, and scintillation photons were detected using a photomultiplier tube (PMT). Scintillation signals were fed to the photon-counting unit and then to a peripheral component interconnect (PCI)-type counting board in a personal computer. Scintillation signals were recorded as a function of time from the difference between trigger and scintillation signals, then the scintillation lifetime was obtained.

Light yields were evaluated using our original setup.[35] The light yield is an important parameter that determines the efficiency of the scintillating material in actual device applications. The glass samples were excited with α-rays from a ^{241}Am source to obtain pulse height spectra. The scintillation signals generated by ^{241}Am α-rays were detected using a PMT (R7600-200, Hamamatsu). The glass samples were optically coupled with the PMT by optical grease (TSK5353, OKEN). The signal generated from the PMT was fed to a preamplifier (113, ORTEC), a shaping amplifier (570, ORTEC), and a multichannel analyzer (8000A, Amptek).

3. Results and Discussion

Figure 1 shows the appearance of all the glass samples. All glass samples appeared transparent under white LED room light. The 0.5% Ce-doped glass sample appeared pale yellow to the naked eye. We summarized the densities of the glass samples in Table 1, which showed a slight increase with increasing concentration of Ce added. Although the concentration of the dopant was small, a significant effect on the glass sample density was observed. As is the case with the results in this study, it was reported that Ce doping increased the density of a Li_2O-Gd_2O_3-BaO-B_2O_3 glass sample.[36] The 0.5% Ce-doped glass sample has a high density, which is comparable to those of Tl:CsI and Ce:Y_2SiO_5 scintillators.[37]

The PL excitation/emission contour map of the 0.1% Ce-doped glass sample, which has the highest *QY* among the glass samples (described below), is shown in Fig. 2. We obtained only one broad emission from 350 to 550 nm under 340 nm excitation. Figure 3 shows the PL excitation/emission contour map of the undoped glass sample. In this sample, we obtained only one emission line at 310 nm under less than 300 nm excitation. The emission line did not appear in the Ce-doped glass samples. We summarized the *QY* values of all the glass samples in Table 2. The 0.1% Ce-doped glass sample showed the highest *QY*, as indicated in the table. The obtained *QY* increased with increasing concentration of Ce, but in the 0.5% Ce-doped glass sample, *QY* was decreased. This phenomenon can be understood in terms of typical concentration quenching.

Fig. 1. (Color online) Photograph of all the glass samples under LED light.

Table 1
Ce concentrations and densities of all the glass samples.

Ce concentration (%)	Density (g/cm^3)
0.5	4.15
0.1	4.14
0.05	4.05
0.01	4.03
0	4.02

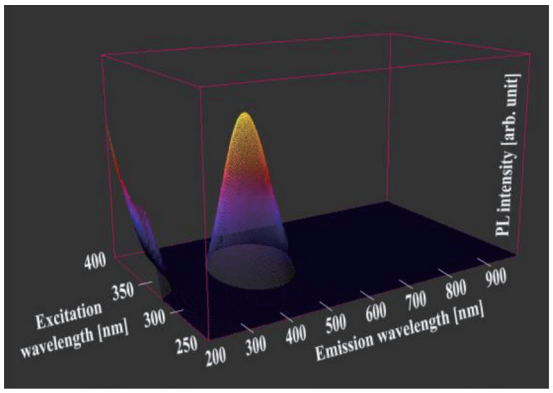

Fig. 2. (Color online) PL excitation/emission contour map of 0.1% Ce-doped glass sample.

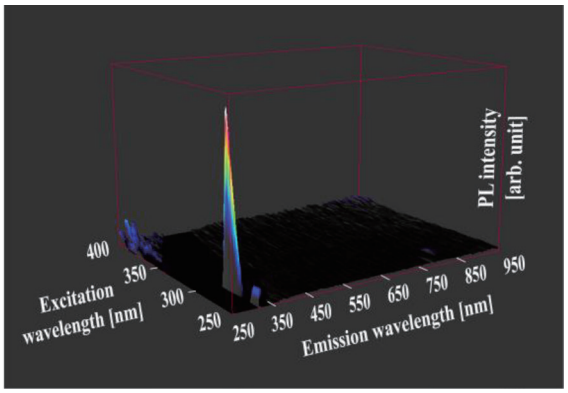

Fig. 3. (Color online) PL excitation/emission contour map of undoped glass sample.

Table 2
PL *QY*s of all the glass samples under 340 nm excitation.

Ce concentration (%)	*QY* (%)
0.5	14.8
0.1	27.9
0.05	26.6
0.01	23.9

The absorption spectra of the glass samples have characteristic absorption bands in the UV region, as shown in Fig. 4. From 400 nm to an infrared wavelength, no significant absorption features were detected. The characteristic absorptions of the sample at 312, 306, 275, 253, and 246 nm are attributed to 4f–4f transitions of Gd^{3+} ions. The absorption peaks at 306 and 312 nm are attributed to the $^8S_{7/2}$–$^6P_{5/2}$ and $^8S_{7/2}$–$^6P_{7/2}$ transitions, respectively.[38,39] In addition, the line at 275 nm is attributed to the $^8S_{7/2}$–$^6I_{7/2}$ transition.[40] Furthermore, the absorptions at 246 and 253 nm are attributed to the $^8S_{7/2}$–$^6D_{7/2}$ and $^8S_{7/2}$–$^6D_{9/2}$ transitions, respectively.[40,41] On the other hand, Ce-doped glass samples have a broad absorption in the whole UV region. Hence, it is reasonable to consider that this absorption bands are due to Ce. The absorption at around 300–350 nm is attributed to Ce^{3+} ions according to the PL excitation/emission contour map. Furthermore, Ce^{4+} ion have a characteristic absorption spread in the whole UV region attributed to charge transfer between O_2 and Ce^{4+}.[42] This is the reason why the glass sample with a high Ce concentration was colored. The emission peak of Gd^{3+} ions overlapped with the absorption bands of Ce^{3+} and Ce^{4+} ions, and this condition was a requirement for the energy transfer between Gd^{3+} and Ce^{3+} to occur.

Figure 5 shows the PL lifetime properties of the emissions observed at 310 and 390 nm. The excitation wavelengths were 253 and 280 nm against the 310 and 390 nm emissions, respectively. In the case of 253 nm excitation, the lifetimes decreased with increasing Ce concentration. Figure 5(a) shows the decay curves focusing on the $^6P_{7/2}$–$^8S_{7/2}$ transition of Gd^{3+} ions at 313 nm. The lifetime of the undoped glass sample was 1.86 ms, which was typical in the $^6P_{7/2}$–$^8S_{7/2}$ relaxation of Gd^{3+} ions. When the Ce concentration increased, the lifetime of

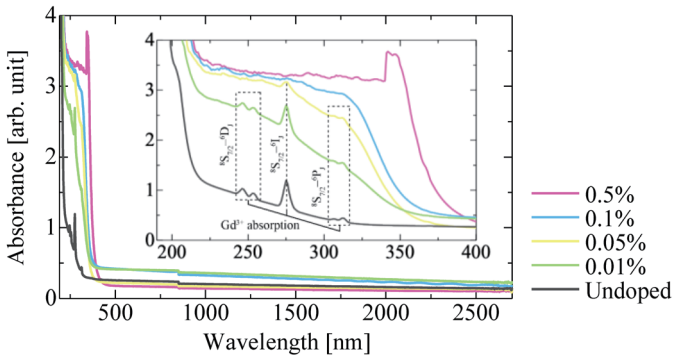

Fig. 4. (Color online) Absorption spectra of all the glass samples. The inset shows an expanded UV range.

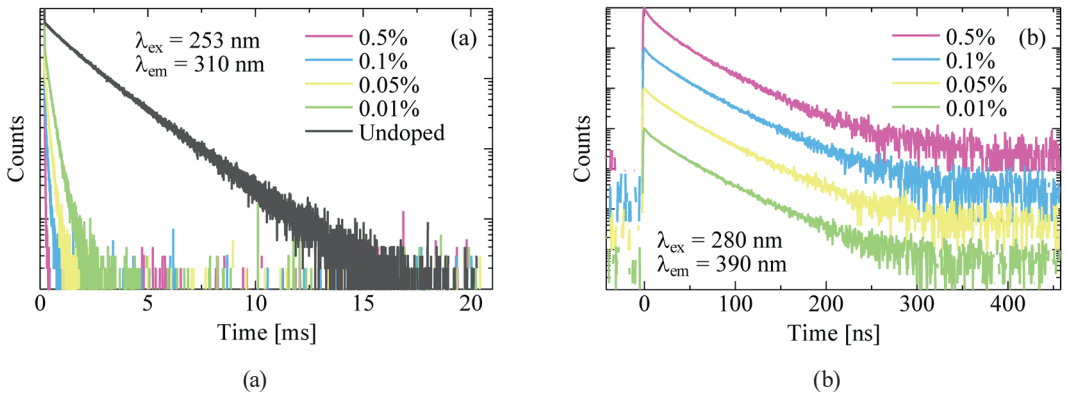

Fig. 5. (Color online) PL lifetimes of glass samples excited with (a) 253 and (b) 280 nm wavelengths.

Gd^{3+} decreased clearly. This trend suggests that energy transfer from Gd^{3+} to Ce^{3+} may occur. Figure 5(b) shows the decay curve of the 5d–4f optical transition of Ce^{3+} ions at around 390 nm. We summarized the calculated lifetimes from Fig. 5(b) in Table 3. These calculated values are characteristics of 5d–4f transitions of Ce^{3+} ions, and the 0.1% Ce-doped glass sample showed the longest lifetime among the glass samples. The fluctuation tendency of the PL lifetimes was consistent with the tendency of *QY*.

Figure 6 shows the X-ray-induced scintillation spectra of the undoped and Ce-doped glass samples. The inset of Fig. 6 focuses on the scintillation at around 400 nm. In the undoped sample, we observed a strong emission line attributed to the $^8S_{7/2}$–^6I_J transition of Gd^{3+} ions at 310 nm and a broad emission from 300 to 600 nm. In contrast, all the Ce-doped glass samples have different tendencies of emissions from the undoped one. The emission intensity due to Gd^{3+} decreased with increasing Ce concentration. This tendency is typical if we assume an energy transfer from Gd^{3+} to Ce^{3+}. Generally, the requirements of energy transfer are (i) a spectral overlap of the emission of the donor (in this case, Gd^{3+}) and the absorption of the acceptor (Ce^{3+}), (ii) a reduction in the lifetime of the donor when the acceptor concentration increases, (iii) an increase in the rise time of the acceptor when the concentration of the acceptor

Table 3
PL lifetimes of Ce-doped glass samples under 280 nm excitation.

Ce concentration (%)	PL lifetime (ns)
0.5	36.8
0.1	39.4
0.05	37.7
0.01	36.8

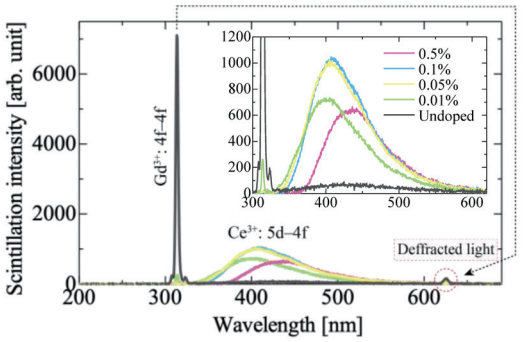

Fig. 6. (Color online) X-ray-induced scintillation spectra of all glass samples. The inset focuses on the emission of Ce^{3+}.

increases, and (iv) an inversely proportional relationship of the emission intensities of the donor and acceptor. Except for (iii), the requirements of the energy transfer are satisfied, and we consider that energy transfer can occur in our glasses. Generally, (iii) is difficult to measure, and a slow rise is not common in materials exhibiting energy transfer. In addition, the emission peaks shifted to the longer wavelength side with increasing Ce concentration. This peak shift is caused by self-absorption with Ce^{4+} ions.

Figure 7 shows the X-ray-induced scintillation lifetimes of all the glass samples, and the calculated lifetimes are shown in Table 4. We observed only the instrumental response function (IRF) and one lifetime of luminescence from the undoped glass sample. This suggests that the undoped glass sample has one emission origin when it is excited by X-rays in this time range. The Ce-doped glass samples indicated two lifetime components excluding the IRF component. The first lifetime component is attributed to emission by the 5d–4f transition of Ce^{3+}, and the lifetime increased with the Ce concentration. From the PL lifetime of Gd^{3+}, energy transfer from Gd^{3+} to Ce^{3+} was observed to occur more strongly at higher Ce concentrations. This suggests that the increase in Ce concentration shortens the distance between Gd and Ce and induces energy transfer more frequently. Namely, introducing Gd into the glass is one of the effective ways to enhance the scintillation efficiency at higher Ce concentrations. These lifetimes were longer than that from PL decay curves. The origin of the second component would be ascribed to defects in the glass host, and the second lifetime component also increased with the concentration of Ce doped since the defects in the glass samples would be amplified by Ce doping.

The 0.1 and 0.5% Ce-doped glass samples showed full energy peaks when irradiated with α-rays from ^{241}Am, as shown in Fig. 8. When we fitted the spectrum of the 0.5% Ce-doped glass sample by a single Gaussian, the peak channel was 235 ch. We estimated the light yield of the 0.5% Ce-doped glass sample on the basis of that of Ce^{3+}:^{6}Li glass [GS-20: $4Ce_2O_3$-$18Li_2O$-$18Al_2O_3$-$4MgO$-$56SiO_2$ (wt%)] under the irradiation of neutrons. The calculated value was 30 ph/MeV (Ce^{3+}:^{6}Li glass: 845 ph/MeV) under α-ray irradiation.

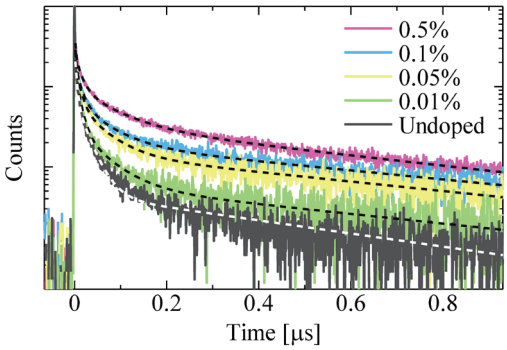

Fig. 7. (Color online) X-ray-induced scintillation lifetimes of all glass samples.

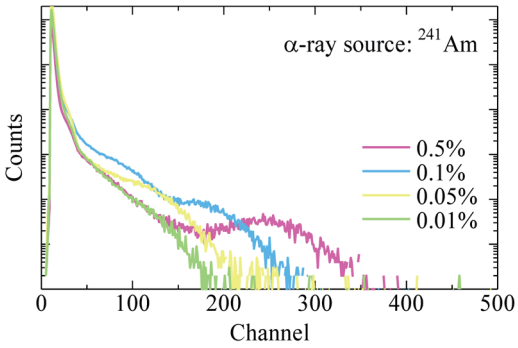

Fig. 8. (Color online) ^{241}Am-excited pulse height spectra of Ce-doped glass samples.

Table 4
X-ray-induced scintillation lifetimes of undoped and Ce-doped glass samples.

Ce concentration (%)	Scintillation lifetime (ns)		
	1st	2nd	3rd
0.5		79.7	679.5
0.1		64.2	723.1
0.05	IRF	55.0	740.5
0.01		58.3	723.1
0		N/A	304.9

4. Conclusions

We synthesized Ce-doped 20BaO-15Gd_2O_3-65SiO_2 glasses. The $^6P_{7/2}$–$^8S_{7/2}$ relaxation of Gd^{3+} was confirmed notably in the undoped glass sample, but the emission disappeared upon the addition of Ce. Furthermore, the decay time constant of Gd^{3+} tended to decrease with increasing Ce concentration. This result suggests that energy transfer from Gd^{3+} to Ce^{3+} occurred in this sample. We observed full energy peaks from pulse height spectra, which proved that Ce-doped 20BaO-15Gd_2O_3-65SiO_2 glasses could work as a scintillation detector.

Acknowledgments

This work was supported by Grants-in-Aid for Scientific Research A (17H01375) and B (18H03468 and 19H03533), Young Scientists B (17K14911), and Early-Career Scientists (18K14158) from JSPS. The Cooperative Research Project of Research Institute of Electronics, Shizuoka University, Iketani Foundation, Murata Foundation, and Nippon Sheet Glass Foundation are also acknowledged.

References

1 C. L. Melcher and J. S. Schweitzer: Nucl. Instrum. Methods Phys. Res., Sect. A **314** (1992) 212.
2 P. Lecoq: Nucl. Instrum. Methods Phys. Res., Sect. A **809** (2016) 130.
3 W. W. Moses: Nucl. Instrum. Methods Phys. Res., Sect. A **487** (2002) 123.

4 W. W. Moses: Nucl. Instrum. Methods Phys. Res., Sect. A **471** (2001) 209.
5 D. Nakauchi, G. Okada, Y. Fujimoto, N. Kawano, N. Kawaguchi, and T. Yanagida: Phys. Chem. Glasses-B **60** (2019) 10.
6 T. Yanagida: P. Jpn. Acad. B-Phys. **94** (2018) 75.
7 I. Ogawa, R. Hazama, H. Miyawaki, S. Shiomi, N. Suzuki, Y. Ishikawa, G. Kunitomi, Y. Tanaka, M. Itamura, K. Matsuoka, S. Ajimura, T. Kishimoto, H. Ejiri, N. Kudomi, K. Kume, H. Ohsumi, and K. Fushimi: Nucl. Phys. A **730** (2004) 215.
8 N. J. C. Spooner, G. J. Davies, J. D. Davies, G. J. Pyle, T. D. Bucknell, G. T. A. Squier, J. D. Lewin, and P. F. Smith: Phys. Lett. B **321** (1994) 156.
9 M. Kole, M. Chauvin, Y. Fukazawa, K. Fukuda, S. Ishizu, M. Jackson, T. Kamae, N. Kawaguchi, T. Kawano, M. Kiss, E. Moretti, M. Pearce, S. Rydström, H. Takahashi, and T. Yanagida: Nucl. Instrum. Methods Phys. Res., Sect. A **770** (2015) 68.
10 H. Takahashi, T. Yanagida, D. Kasama, T. Ito, M. Kokubun, K. Makishima, T. Yanagitani, H. Yagi, T. Shigeta, and T. Ito: IEEE Trans. Nucl. Sci. **53** (2006) 2404.
11 J. Glodo, Y. Wang, R. Shawgo, C. Brecher, R. H. Hawrami, J. Tower, and K. S. Shah: Phys. Procedia **90** (2017) 285.
12 V. D. Ryzhikov, A. D. Opolonin, P. V. Pashko, V. M. Svishch, V. G. Volkov, E. K. Lysetskaya, D. N. Kozin, and C. Smith: Nucl. Instrum. Methods Phys. Res., Sect. A **537** (2005) 424.
13 L. E. Sinclair, D. S. Hanna, A. M. L. MacLeod, and P. R. B. Saull: IEEE Trans. Nucl. Sci. **56** (2009) 1262.
14 C. Tang, S. Liu, L. Liu, and D. P. Chen: J. Lumin. **160** (2015) 317.
15 K. D. Ianakiev, M. P. Hehlen, M. T. Swinhoe, A. Favalli, M. L. Iliev, T. C. Lin, B. L. Bennett, and M. T. Barker: Nucl. Instrum. Methods Phys. Res., Sect. A **784** (2015) 189.
16 N. Kawaguchi and T. Yanagida: Sens. Mater. **31** (2019) 1257.
17 D. Shiratori, Y. Isokawa, N. Kawaguchi, and T. Yanagida: Sens. Mater. **31** (2019) 1281.
18 N. Kawano, N. Kawaguchi, G. Okada, Y. Fujimoto, and T. Yanagida: Sens. Mater. **30** (2018) 1539.
19 H. Fukushima, D. Nakauchi, N. Kawaguchi, and T. Yanagida: Sens. Mater. **31** (2019) 1273.
20 Y. Fujimoto, K. Saeki, D. Nakauchi, T. Yanagida, M. Koshimizu, and K. Asai: Sens. Mater. **30** (2018) 1577.
21 W. Chewpraditkul, Q. Sheng, D. Chen, A. Beitlerova, and M. Nikl: Phys. Status Solidi **209** (2012) 2578.
22 W. Chewpraditkul, X. He, D. Chen, Y. Shen, Q. Sheng, B. Yu, M. Nikl, R. Kucerkova, A. Beitlerova, C. Wanarak, and A. Phunpueok: Phys. Status Solidi **208** (2011) 2830.
23 Q. Wang, B. Yang, Y. Zhang, H. Xia, T. Zhao, and H. Jiang: J. Alloy. Compd. **581** (2013) 801.
24 M. Rodová, A. Cihlář, K. Knížek, K. Nitsch, and N. Solovieva: Radiat. Meas. **38** (2004) 489.
25 J. Fu, J. M. Parker, R. M. Brown, and P. S. Flower: J. Non. Cryst. Solids **326**–**327** (2003) 335.
26 M. Nikl, K. Nitsch, E. Mihokova, N. Solovieva, J. A. Mares, P. Fabeni, G. P. Pazzi, M. Martini, A. Vedda, and S. Baccaro: Appl. Phys. Lett. **77** (2000) 2159.
27 Y. Isokawa, D. Nakauchi, G. Okada, N. Kawaguchi, and T. Yanagida: J. Alloy. Compd. **782** (2019) 859.
28 Y. Isokawa, H. Kimura, T. Kato, N. Kawaguchi, and T. Yanagida: Opt. Mater. **90** (2019) 187.
29 N. Kawaguchi and T. Yanagida: Sens. Mater. **31** (2019) 1257.
30 H. Masai, G. Okada, N. Kawaguchi, and T. Yanagida: Opt. Mater. **88** (2019) 1.
31 G. Okada, S. Kasap, and T. Yanagida: J. Ceram. Soc. Jpn. **124** (2016) 541.
32 G. Okada, S. Kasap, and T. Yanagida: Opt. Mater. **61** (2016) 15.
33 T. Yanagida: Opt. Mater. **35** (2013) 1987.
34 T. Yanagida, Y. Fujimoto, T. Ito, K. Uchiyama, and K. Mori: Appl. Phys. Express **7** (2014) 062401.
35 D. Nakauchi, N. Kawaguchi, and T. Yanagida: Sens. Mater. **31** (2019) 1249.
36 F. Zaman, G. Rooh, N. Srisittipokakun, H. J. Kim, E. Kaewnuam, P. Meejitpaisan, and J. Kaewkhao: Radiat. Phys. Chem. **130** (2017) 158.
37 B. Liu and C. Shi: Chinese Sci. Bull. **47** (2002) 1057.
38 V. Jubera, J. Chaminade, A. Garcia, F. Guillen, and C. Fouassier: J. Lumin. **101** (2003) 1.
39 M. Xu, L. Wang, L. Liu, D. Jia, and R. Sheng: J. Lumin. **146** (2014) 475.
40 W. Chewpraditkul, N. Pattanaboonmee, N. Yawai, W. Chewpraditkul, P. Lertloypanyachai, K. Sreebunpeng, M. Yoshino, L. Liu, and D. Chen: Opt. Mater. (2019) 109468.
41 D. He, C. Yu, J. Cheng, S. Li, and L. Hu: J. Rare Earth **29** (2011) 48.
42 L. S. Živković, V. Lair, O. Lupan, M. Cassir, and A. Ringuedé: Acta Phys. Pol. A **120** (2011) 298.